

# Sympathetic ground state cooling and coherent manipulation with two-ion-crystals

H. Rohde, S. T. Gulde, C. F. Roos, P. A. Barton, D. Leibfried,  
J. Eschner, F. Schmidt-Kaler §, and R. Blatt

Institut für Experimentalphysik, Universität Innsbruck, Technikerstrasse 25, A-6020  
Innsbruck, Austria

**Abstract.** We have cooled a two-ion-crystal to the ground state of its collective modes of motion. Laser cooling, more specific resolved sideband cooling is performed sympathetically by illuminating only one of the two  $^{40}\text{Ca}^+$  ions in the crystal. The heating rates of the motional modes of the crystal in our linear trap have been measured, and we found them considerably smaller than those previously reported by Q. Turchette *et. al.* Phys. Rev. A 61, 063418 (2000) in the case of trapped  $^9\text{Be}^+$  ions. After the ground state is prepared, coherent quantum state manipulation of the atomic population can be performed. Within the coherence time, up to 12 Rabi oscillations are observed, showing that many coherent manipulations can be achieved. Coherent excitation of each ion individually and ground state cooling are important tools for the realization of quantum information processing in ion traps.

## 1. Introduction

The coherent control of quantum systems has been given much attention and experimental effort in recent years. In particular, there has been a concerted effort in developing the experimental tools needed to create scalable quantum information processing (QI), and in smaller ‘proof of principle’ demonstrations of QI. The use of the quantum systems at the heart of these experiments relies on the entanglement between subsystems. This might be easily destroyed by the coupling to the environment. As a suggestion for a well controllable, almost decoherence-free system with which to realise a quantum computer, a linear ion trap was proposed by Cirac and Zoller [1]. Indeed, this idea seems so promising at present that many groups are actively pursuing research towards quantum state preparation and manipulation in ion traps. [2, 3, 4, 5, 6, 7]

The Cirac & Zoller scheme uses the internal states of a chain of trapped ions as qubits. Each of these ions represents a qubit and needs to be manipulated separately and distinctly with laser light [8]. Ions in the chain are then coupled by the laser excitation of vibrational modes of the crystal within the trapping potential. As this quantum of motion is common to all of the ions, it acts as a so called ‘quantum bus’ (gate mode), transporting information in the chain of ions. In order to implement the

§ e-mail: Ferdinand.Schmidt-Kaler@uibk.ac.at

Cirac & Zoller proposal for a quantum gate, the gate mode must be prepared in the ground state prior to the gate operation. Cooling of ion crystals has been previously demonstrated [9]. This technique is not only important for ion trap QI's but also in frequency measurements on chains of ions [10] and in QED experiments with trapped ions.

So far, cooling to the motional ground state has been performed only on  $^9\text{Be}^+$  two-ion-crystals by illuminating the entire ion chain [2, 9]. In our experiment, we have pre-cooled two-ion-crystals into the mK range by laser cooling (Doppler cooling) and identified all motional eigenmodes. Then, we have cooled the two-ion-crystal to the vibrational ground state by illuminating only one of the two ions (sideband cooling). Thus we present here the first demonstration of sympathetic ground state cooling of an ion string. If we cool only *one of the eigenmodes*, we achieve a ground state population of any of the modes which is greater than 95%. The other modes are left in their thermal states. However, the fidelity of coherent manipulation of the ion's quantum state would be spoiled due to the thermal distribution of the other modes.

Sequentially we have cooled *all eigenmodes* and we achieve a greater than 95% ground state population of the axial mode (gate mode) and a phonon number between 1 and 2 for the other modes ('spectator' modes). After that, coherent manipulation of the ions' state is possible. We choose two levels, the  $S_{1/2}$  ground state and the long lived  $D_{5/2}$  metastable state, for the qubit basis for QI processing. In our experiment, we demonstrate how each of the ions' state can be manipulated ("single qubit rotation"). The coherence of this optical state manipulation is shown by 12 Rabi oscillations with better than 60% contrast.

We measure heating rates of the vibrational eigenmodes and find they are all well below 20 phonons  $\text{s}^{-1}$ . This slow heating rate, in combination with the sympathetic cooling method, will be of importance for QI: Recent proposals suggesting continuous sympathetic ground state cooling together with coherent manipulation of qubits at different locations in the ion string [11, 12] appear no longer unrealistic in view of these findings.

## 2. The experiment

In our experiments we confine  $^{40}\text{Ca}^+$  ions in a linear Paul trap [3]. Four stainless steel rods of 0.6 mm diameter are arranged parallel at the corners of a square shape of side of length 2.1 mm. The direction of the rods defines the axial symmetry of the trap (fig. 1, left). An alternating radio frequency (rf) field is applied to two diagonally located rods while both the other rods are held at zero volts. In such a way, an electric quadrupole field along the axial direction is generated which provides radial confinement for a charged particle if the rf-frequency and amplitude is chosen properly [13]. Two stainless steel endcap rings of inner diameter 6.7 mm spaced 10 mm apart over the rods are charged with a positive voltage which provides axial confinement (fig. 1, left). The electrode arrangement is held together using isolating macor spacers (not shown

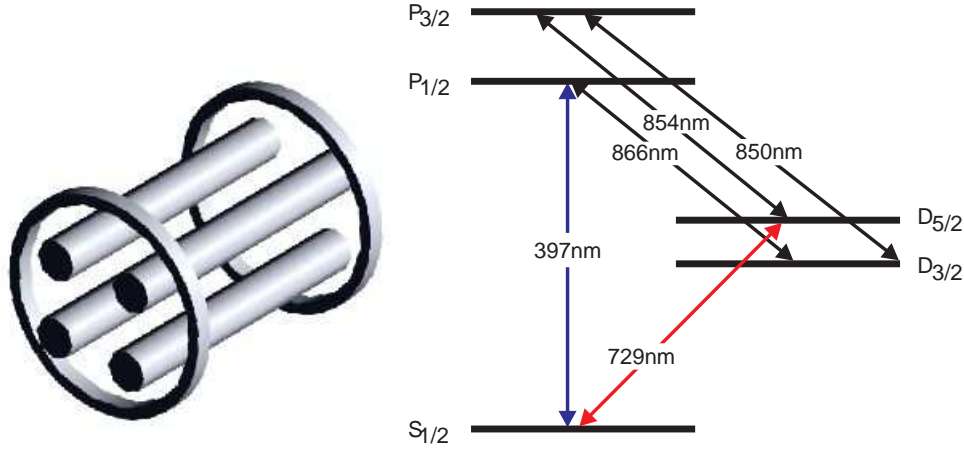


**Figure 1.** Left: A figure of the trap showing the ring endcaps and the four rf electrodes. Right:  $^{40}\text{Ca}^+$  level scheme. Only relevant levels and their transition wavelengths are shown.

in the figure) which assure a  $20\ \mu\text{m}$  tolerance in the position of the four rods and the endcap electrodes. The trap is housed in a vacuum chamber with a pressure less than  $10^{-10}$  mbar.

The rf voltage applied to the rods is produced by resonantly enhancing a source ( $\omega_{rf} = 16.0$  MHz and typical power 4 W) in a helical resonator (loaded  $Q \approx 250$ ). These parameters lead to an rf voltage of about  $300\ \text{V}_{rms}$  and typical radial secular frequencies of  $\omega_{rad} = 1.8$  MHz. The radial x- and y-directions (orthogonal to the axial direction) are degenerate in frequency. For axial confinement, we apply a DC voltage to the ring shaped endcap electrodes (fig. 1, left). For the typical trapping operation we use 2 kV which gives an axial secular frequency of  $\omega_{ax} = 700$  kHz. With this ratio of radial and axial frequency, crystals with up to 5 ions arrange themselves in a linear string. Ions are generated by electron bombardment of a weak neutral Ca atomic beam, and loaded into the trap. This loading process also generates electric stray voltages, shifting the ions out of the trap centre, which is the rf field node line, and resulting in a driven 'micro'-motion of the chain. We compensate for the stray charges using the following procedure: With laser beams at 397 nm from different directions the residual micromotion is detected in the respective directions via the modulation of the fluorescence rate, induced by the Doppler shift of the moving ions [14] and the micromotion is nulled by the application of well chosen voltages on additional compensation electrodes. Due to the slight asymmetries of the trap construction, a compensation voltage dependent on the endcap DC voltage is required. In addition, due to the stray charges (possibly on the macor surfaces of the trap arrangement), we need compensation voltages which vary from load to load. Furthermore, these stray charges leak away within a timescale of hours which requires frequent recompensation. Once compensated, linear ion string configurations lie on the rf node line, thus having no micromotion, which is of great importance for cooling (see sect. 3) and coherent

manipulation of the qubit transition, as far as QI processing is concerned.

Since a single trapped particle has three normal modes of motion, the two-ion-crystal vibration is described by 6 vibrational modes [15, 16] : Three centre of mass modes (of which one is axial and two are radial) at  $\omega_{ax}$  and  $\omega_{rad}^{(x,y)}$  respectively, two 'rocking' modes at  $\omega_R^{(x,y)} = (\omega_{rad}^{(x,y)2} - \omega_{ax}^2)^{1/2}$  (where the atoms swing in opposite directions radially) and the 'breathing' mode (where the two ions oscillate exactly out of phase along the axial direction) at  $\omega_b = \sqrt{3} \omega_{ax}$ . In the specific case of this trap, the radial x- and y-oscillation frequencies are degenerate, giving rise to four distinct normal mode frequencies in total.

We trap  $^{40}\text{Ca}^+$  ions (relevant energy levels shown in figure 1, right). All the necessary wavelengths of light can be generated using solid state lasers and frequency doubling techniques [3]. Light at a wavelength of 397 nm is produced by frequency doubling a stabilized Ti:Sapphire laser (linewidth  $< 300$  kHz). Using the  $S_{1/2} \rightarrow P_{1/2}$  transition, we perform conventional Doppler cooling and detect the ions resonance fluorescence on an intensified CCD camera and a photomultiplier. The  $P_{1/2}$  state may decay with a branching ratio of 1/15 into the metastable  $D_{3/2}$  state, so a diode laser at 866 nm is used to repump the population back via the  $P_{1/2}$  state. A second diode laser at 854nm can be used to remove the population in the  $D_{5/2}$  state via a transition to the  $P_{3/2}$  state. The quadrupole transition near 729 nm connects the  $S_{1/2}$  electronic ground state to the metastable  $D_{5/2}$  state (lifetime  $\sim 1$  s). The  $S_{1/2}$  to  $D_{5/2}$  quadrupole transition at 729 nm is excited with a highly stable Ti:Sapphire laser (linewidth  $< 100$  Hz). This transition is used for the implementation of the two logic states of the qubit: We can detect whether a transition to  $D_{5/2}$  occurred by applying the beams at 397 nm and 866 nm and monitoring the fluorescence of the ion. In 12 ms we typically collect 30 fluorescence photons per ion on a stray light background of 10 photons if the ion is in the electronic ground state [21]. The internal state of the ion can thus be discriminated with an efficiency above 98% [23].

### 3. Doppler cooling

After Doppler cooling, the ion cloud crystallizes into a linear string, thus performing the initial cooling step towards the motional ground state [18]. Optimum Doppler cooling is achieved at a laser frequency of  $\delta\omega = -\Gamma/2$ , red detuned from the resonance, and leads to a temperature in the mK regime, with the natural linewidth of the  $S_{1/2} \rightarrow P_{1/2}$  transition being  $\Gamma = 20$  MHz. In the case of one cooling laser beam, with optimum detuning and incident parallel to the oscillator axis, the Doppler cooling limit is given as  $k_B T = \frac{1}{2} \hbar \Gamma$ .

In our specific case, at least a number of additions to the above simple picture affect the cooling limit: (i)  $^{40}\text{Ca}^+$  is not a true two-level-system since both the  $S_{1/2} \rightarrow P_{1/2}$  at 397 nm and the  $D_{3/2} \rightarrow P_{1/2}$  transition at 866 nm have to be excited for Doppler cooling. As shown, for example, in ref. [17] this leads to coherent superposition states of the  $S_{1/2}$  and the  $D_{3/2}$  state ('dark resonances'), which can increase or decrease the Doppler

cooling limit, depending on the relative detuning of both laser frequencies. Since dark resonances can exhibit spectral features much narrower than the natural linewidth, the detuning of the lasers strongly influences the cooling. (ii) We apply a magnetic field of 3.6 Gauss (to generate a quantization axis), which leads to a frequency splitting of all Zeeman substates. With the two laser beams at 397 nm we simultaneously drive  $\pi$ -transitions and  $\sigma^- / \sigma^+$ -transitions. Thus, four resonances between the  $S_{1/2}, m_J = \pm 1/2$  manifold and  $P_{1/2}, m_J = \pm 1/2$  manifold are excited, all of them slightly shifted against each other in frequency due to different Landé factors, which leads to an effective broadening of the cooling transition. For example, the  $\sigma^-$  and the  $\sigma^+$ -transitions are split by  $\approx 13$  MHz. The laser detuning can no longer be optimally chosen for Doppler cooling with respect to *all transitions* between the Zeeman substates  $m_J = \pm 1/2$ . (iii) Residual micromotion of the trapped ions leads to a larger cooling limit. With a rf drive frequency of 16 MHz, the micromotion modulates the bare spectral line, generating resonances ('sidebands') which are not resolved under the natural linewidth of the  $S_{1/2} \rightarrow P_{1/2}$  transition. These unresolved micromotion components broaden the cooling transition. (iv) We try carefully to avoid any saturation of the cooling transition which would lead to further broadening.

Due to the combination of reasons (i) to (iv), we can explain the somewhat larger width of the observed excitation spectrum on the  $S_{1/2} \rightarrow P_{1/2}$  transition of  $\Gamma_{exp} \approx 30$  MHz. (v) It seems that intrinsic heating processes do not play any role if we assume the measured heating rates for the ground state (see section 7) to be approximately valid also at higher phonon numbers,  $\bar{n}$ . (vi) The limit of Doppler cooling can always be expressed as the balance between cooling processes and heating processes. If the laser beam direction is not parallel with the oscillator axis, but has an angle with respect to the oscillator axis, the probability for the cooling process decreases, while the heating process (by spontaneous emission) is independent of the beam direction. As a result, the cooling limit is increased: For our experimental arrangement with two laser beams, and taking into account the angles between these cooling beams and the principal trap axes, we estimate that in the axial motional mode a cooling is reached which corresponds to a mean phonon number of  $\bar{n}_{axial} = 45(10)$  and  $\bar{n}_{radial} = 40(10)$ . For the calculation of these phonon numbers, we have taken the effective linewidth of 30 MHz into account. The uncertainty is caused by imprecise knowledge of the exact fraction of light power going to each of the cooling beams and their exact focus sizes. Spectroscopy on the  $S_{1/2} \rightarrow D_{5/2}$  transition (as will be discussed in the next section) yields 50(10) in the radial, and 45(10) phonons in the axial direction.

#### 4. Spectroscopy of the $S_{1/2}$ - $D_{5/2}$ transition

For coherent spectroscopic investigation and state engineering on the  $S_{1/2} \leftrightarrow D_{5/2}$  transition at 729 nm we use a pulsed technique which consists of four consecutive steps. (i) *Doppler cooling*: Laser light at 397 nm, 866 nm, and 854 nm is used to pump the ion to the  $S_{1/2}$  ground state and pre-cool the vibrational state to a value near the Doppler

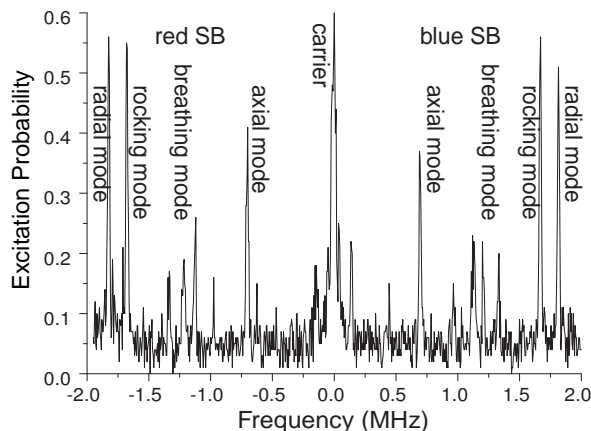


**Figure 2.** Spectrum of a two ion chain, excitation probability is plotted against 729 nm laser detuning. The detuning of the laser is taken to be zero at the carrier frequency. All first order sidebands are named as in the text.

limit. (ii) *Optical pumping*: The  $S_{1/2}(m_J = -1/2)$  sub-state is prepared by optical pumping with  $\sigma^-$  radiation at 397 nm. A magnetic field of 3.6 Gauss at right angles to the direction of the  $k$ -vector of the light at 729 nm provides a quantization axis and splits the 10 Zeeman components of the  $S_{1/2} \leftrightarrow D_{5/2}$  transition in frequency. (iii) *Excitation step*: We excite the  $S_{1/2}(m_J = -1/2) \leftrightarrow D_{5/2}(m = -5/2)$  transition at 729 nm with laser pulses of well controlled frequency, power, and duration. (iv) *State analysis*: We collect the ion's fluorescence under excitation with laser light at 397 nm and 866 nm and detect whether a transition to the shelving level  $D_{5/2}$  has been previously induced.

Sequence (i)-(iv) is repeated 100 times to measure the  $D_{5/2}$  state occupation probability  $P_D$  after step (iii). We study the dependence of  $P_D$  on the experimental parameters such as the detuning  $\delta\omega$  of the light at 729 nm with respect to the ionic transition or the length of one of the excitation pulses in step (iii). The duration of a single sequence is typically 20 ms (in some cases 40 ms), so that we can synchronize the sequence with the ac power line at 50 Hz to reduce the influence of ac magnetic field fluctuations.

The direction of the laser at 729 nm, which is used for spectroscopy, resolved sideband cooling and for individual quantum manipulation, is at 67.5 degrees with respect to the axial direction. The ion-light interaction [19] is described by the Lamb Dicke parameters  $\eta_{ax} = 4.3\%$ ,  $\eta_{rad} = 6.6\%$  for the excitation of the axial and radial sidebands respectively ( $\eta$  being defined as  $k \cos \phi \sqrt{\hbar/2m\omega}$ , where  $\phi$  is the angle between the oscillator axis and the incident laser beam,  $m$  is the mass of the ion crystal and  $\omega$  is the relevant trap oscillator frequency).

The observed excitation spectrum on the  $S_{1/2}(m_J = -1/2) \leftrightarrow D_{5/2}(m_J = -5/2)$  transition (figure 2) consists of the following spectral resonances: First there is an atomic line at the bare frequency of the transition ('carrier'). In addition to this line, there are spectral resonances which are due to the harmonic oscillator frequencies of the ions in

the trap. Thus, the 4 distinct frequencies of motion lead to 4 distinct resonances on the red wavelength side of the central line and symmetrically on the blue wavelength side. In addition to these first order modulations, there are second order modulations of the first order resonances themselves and so forth. This results in a complicated comb structure of sidebands [3]. The width of the comb is dependent on the temperature of the ion chain. With the initial Doppler cooling step we are able to reduce the thermal phonon number in all modes of the two-ion-crystal sufficiently that only a few resonances are strong, a typical spectrum is shown in figure 2 with all first order sidebands named. We denote these resonances as follows: The 'carrier' transition means the phonon number of all motional modes remains the same when the ion undergoes the transition from the  $S_{1/2}$  ground state to the  $D_{5/2}$  state. A red (respectively blue) sideband means that the excitation of the particular mode removes (adds) one phonon when the electronic transition is excited.

Using the calculated Lamb-Dicke parameters in the radial and axial directions, we compare the excitation dynamics on the  $S_{1/2} - D_{5/2}$  transition for the vibrational sidebands, quantified by the population  $P_{D_{5/2}}(t)$  after an excitation time  $t$ , with that on the carrier transition. For a thermal distribution with mean phonon number  $\bar{n}$ , which is characterized by the phonon distribution  $p_n$ , we expect a blue sideband Rabi oscillation of  $P_{D_{5/2}}^{SB}(t) \propto \sum p_n \sin^2(\eta\sqrt{n+1} \cdot t)$ , while for the carrier transition the Rabi oscillation is given by  $P_{D_{5/2}}^{Carrier}(t) \propto \sum p_n \sin^2((1 - \eta^2 n) \cdot t)$  [19]. Thus, from the observation of Rabi oscillations of  $P_{D_{5/2}}(t)$  we are able to deduce the mean phonon number,  $\bar{n}$ , after Doppler cooling (section 3). We typically find for a single Doppler-cooled trapped ion, mean phonon numbers of radial  $\bar{n} = 50(10)$ , and axial  $\bar{n} = 45(10)$ , which indicates that the ions are confined within the Lamb-Dicke regime, with  $\eta\sqrt{\bar{n}} < 1$ .

## 5. Sideband cooling of the two-ion-crystal

After Doppler cooling the two-ion-crystal into the Lamb-Dicke regime, *resolved sideband cooling* is applied in order to cool to the motional ground state. The sideband cooling uses the quadrupole  $S_{1/2}(m_J = -1/2) \leftrightarrow D_{5/2}(m_J = -5/2)$  transition which has a natural linewidth of 0.16 Hz. Only one of the ions is illuminated, and so only the electronic population of one ion is driven although the motional modes are common to both ions. First, the required frequencies have already been determined by spectroscopic investigation as described in section 4. Then the laser at 729 nm is tuned to the red sideband of the mode of motion we wish to cool. With each photon absorbed, the ion-crystal loses one phonon of motional energy of the specific mode. As the lifetime of the  $D_{5/2}$  state is long, the population must be recycled quickly to the lower state, thus the laser at 854 nm is switched on during this sideband cooling pulse, quenching the atomic population in the  $D_{5/2}$  state via the  $P_{3/2}$  state. Subsequent spontaneous decay closes the cooling cycle, but does not change the phonon number as the Lamb-Dicke parameter  $\eta_{393}$  is small. The approximate laser power between 5 to 20 mW at 729 nm is focused to a waist size of 3.7  $\mu\text{m}$ , and the power of the 854 nm (laser focus size: 100

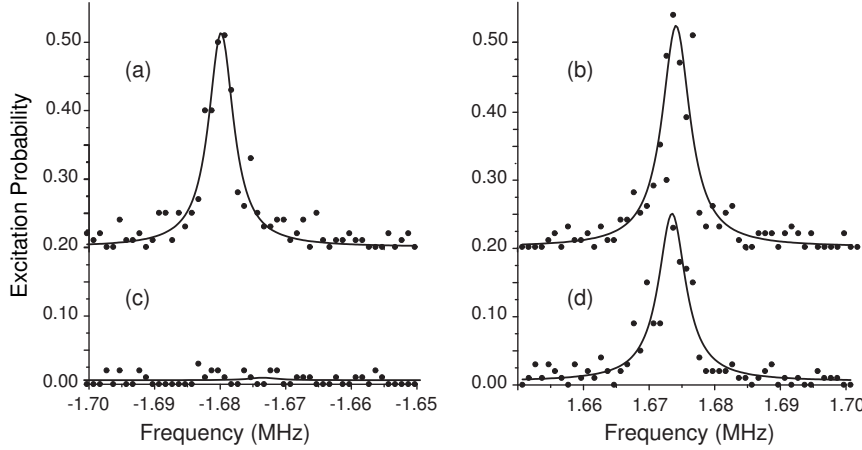


**Figure 3.** Sideband cooling on the  $S_{1/2} - D_{5/2}$  transition for two ions in the linear trap. The radial sideband excitation is shown after Doppler cooling (upper traces a, and b) and after ground state cooling (lower traces c, and d). The y-axis of the upper traces has been offset by 0.2 for clarity. From the asymmetry of red (a, c) and blue sideband excitation (b, d) we deduce a 98.5(1.5)% ground state probability.

to 200  $\mu\text{m}$ ) is adjusted for optimum cooling, typically a few tenths of a mW. The ion is illuminated with both laser fields for a time of 6 ms. Under these operating conditions, we observe efficient red sideband cooling at 729 nm within a bandwidth of 5 kHz. During the cooling and quenching pulse, short pulses of  $\sigma^-$  polarised light are applied. With that, any accidental loss of population into the  $S_{1/2}(m_J = +1/2)$  state is repumped and the ion is returned to the the cooling cycle. The duration of these pulses is kept at a minimum to prevent unwanted heating.

At the end of the cooling phase there is a probe pulse of light at 729 nm followed by detection on the Doppler cooling transition to obtain the motional quantum state. Thus the ground state cooling step is placed between steps (ii) and (iii) of the spectroscopic sequence. The frequency of the 729 nm probe pulse is varied and the spectrum after sideband cooling recorded. Any population in the ground state of a motional mode will not be excited by the probe pulse when tuned to the red sideband and so the strength of this line in the spectrum will be greatly reduced. Measuring the absorption on the red (*rsb*) and blue (*bsb*) sidebands of the cooled mode allows us to determine the ground state population,  $p_0 = 1 - (rsb/bsb)$ .

For cooling only a *single mode of the motion*, one cooling pulse of 6.4 ms is used. This cooling time is chosen such that the mode is cooled to the ground state. We have cooled all of the motional modes separately using the scheme as described. The obtained cooling results show that we are able to reliably cool all modes separately to a ground state population of over 95%. Figure 3 shows the red and blue radial sidebands before and after cooling giving a 98.5(1.5)% ground state probability. We are able to prepare the 1-D zero point of motion of any oscillator that could be used as the 'gate mode' in a realisation of a small QI processor. However, any uncooled modes with thermal



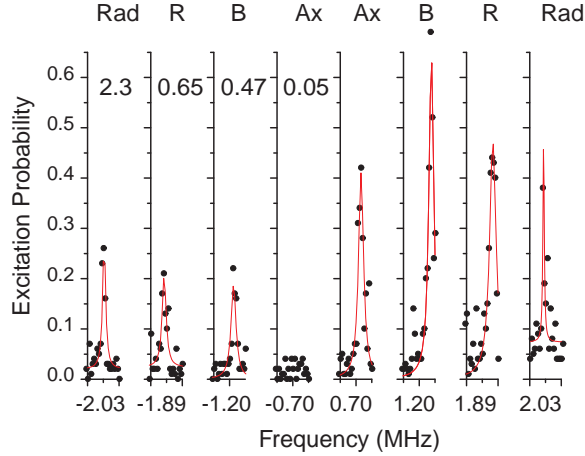


**Figure 4.** Four sideband cooling, excitation probability is plotted against 729 nm laser detuning. The four red and blue motional sidebands are shown after cooling. The points are experimental data with fits to the data shown as solid lines. The residual average phonon numbers in each motional mode are shown. The final ground state population for the axial mode is greater than 95%.

phonon number distributions ('spectator' modes), affect the coherent dynamics on the cooled mode. An approximate expression for the maximum number  $N^*$  of Rabi cycles, is given by  $N^* \leq 1/(2\eta^2\bar{n})$ , where  $\bar{n}$  and  $\eta$  accounts for the mean phonon number and Lamb-Dicke factor of a spectator mode [23]. Thus if the average number of phonons is high in a mode, significantly different Rabi frequencies occur and Rabi oscillations are washed out. Therefore, in order to maximise the possible number of gate operations these spectator modes must also be cooled.

In order to cool *all of the motional modes* such that they are all prepared close to the ground state, we use a scheme almost identical to that above, although during the cooling pulse we clearly need to apply light at all the red sideband frequencies. So, rather than using a single cooling pulse we apply four separate pulses, each 6 ms long, and each tuned to the red sideband of a different oscillator, i.e. radial, rocking, breathing and axial. During each cooling pulse the quenching and repumping lasers are also applied, and once again only one ion is illuminated. The power of the cooling laser at 729 nm of each pulse is chosen to optimise cooling results. Cooling is applied in the following order: radial, rocking, breathing and axial. Since we intend to use the axial motional mode as the gate mode, this is the last to be cooled (with the lowest residual phonon number). After cooling, the population is once again probed, and the spectrum of all four motional modes is recorded. In figure 4 the red and blue sidebands of all four motional modes are shown after cooling. In stark contrast to the sidebands before cooling (in figure 2 the red and blue sidebands are of approximately the same height) those on the red side have all but disappeared. For the scan shown in figure 4 this reveals the following average phonon numbers,  $\bar{n} = p_0^{-1} - 1$ , for each mode: radial  $\bar{n}_{rad} = 2.3$ , rocking  $\bar{n}_R = 0.65$ , breathing  $\bar{n}_b = 0.47$  and axial  $\bar{n}_{ax} = 0.05$ .

Trap	Mode	Frequency (MHz)	1/e time (ms)	to 1 phonon (ms)
Linear	breathing	1.2	3.2	4.0
Linear	rocking	1.7	1.2	3.0
Spherical, single ion	axial	4	0.2	$\leq 0.2$
Spherical, single ion	radial	1.9		

**Table 1.** Cooling times for various motional modes, for the spherical trap see [23, 4].

As follows from the above discussion, we see that (i) the axial gate mode phonon number is indeed well prepared for the implementation of a cold gate, e.g. of Cirac & Zoller type, and (ii) the low phonon number of the spectator modes allows for high contrast Rabi cycles since  $\eta^2 \bar{n} \ll 1$ .

## 6. Cooling times and heating rates

Aside from the purity of preparation of the motional ground state, the dynamics of cooling and heating is important. We thus investigate the cooling and heating rates of the various modes of motion. For the cooling rate, we vary the cooling time,  $t_{cool}$ , and measure the residual phonon number of the respective mode as described earlier for the sideband cooling. The remaining phonon number in the mode is then plotted against the cooling time and characteristic times can be deduced. The result is given as the time to reach  $1/e$  of the initial phonon number (see figure 5 and table 1). A second measure, mainly important for the spectator modes, is the time which is necessary for reaching a mean phonon number near one, corresponding to the state which allows high contrast coherent manipulation with  $\eta^2 \bar{n} \ll 1$ . Of course, the cooling times are a function of the

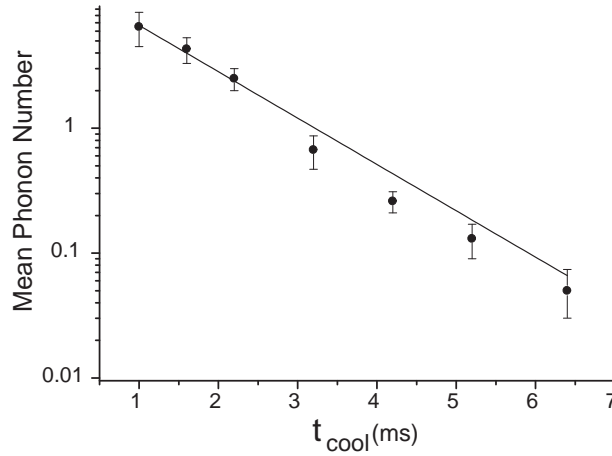


**Figure 5.** Cooling rate of the rocking mode, phonon number is plotted against the duration of the sideband cooling pulse. Points are experimental data with error bars and the line is a fit to the data. The  $1/e$  cooling time is 1.2 ms and over 95% ground state population is achieved at the end of the cooling pulse

laser powers at 729 nm and 854 nm, table 1 gives the values under typical operating conditions. As can be seen from table 1, the characteristic times are all below 4 ms. This shows that with our chosen cooling time of 6 ms per mode we have high ground state occupation probability in all modes and this is largely sufficient to prevent spectator mode decoherence of the coherent dynamics.

To yield the heating rate  $\dot{n}$  of one mode, we first prepare the crystal in its motional ground state and then switch off all laser beams. We let the system evolve freely under the influence of the environment for a delay time  $t_D$ . Using the same method as before we calculate the average phonon number in the mode of interest and plot this value with the delay time, thus we can measure the heating rate. Our measured heating rates for various modes of the collective motion are summarized in table 2. Typical heating rates in the Innsbruck  $\text{Ca}^+$  traps are  $\approx 10\text{-}20$  phonons  $\text{s}^{-1}$ . We have not observed an increase of heating rates over a period of one year, unlike ref. [20], even though the linear trap was found to be heavily coated with Calcium when the vacuum system was opened. In addition, we did not observe a large difference between the heating rates for c.o.m. and other modes.

In order to compare the values of heating rates for the  $\text{Ca}^+$  traps to other measured heating rates in spherical and linear  $\text{Be}^+$  traps [20], we scale the motional heating rates

Ion and Trap	Size $d$ $\mu\text{m}$	Mode	Frequency (MHz)	Heating Rate (phonons/s)	normalized Heating (for 1 MHz)
$^{40}\text{Ca}^+$ , linear	1180	breathing	1.2	10	12
		rocking	1.7	8	14
		radial	1.9	25(10)	47(20)
$^{40}\text{Ca}^+$ , spherical	700	c.o.m, axial	4	5.2	21
		c.o.m, radial	1.9	14	27
$^9\text{Be}^+$ , sph. # 2	175	c.o.m. (x)	8.6	$19\,000^{+40000}_{-13000}$	$160\,000^{+340000}_{-111000}$
		breathing-x	15	$\leq 180$	$\leq 2\,700$
		rocking-xy	15	$\leq 1000$	$\leq 15\,000$
$^9\text{Be}^+$ , sph. # 3b	395	c.o.m.	1.4 - 3.4	varies	5 000
$^9\text{Be}^+$ , lin. # 4	280	c.o.m.	3 - 17	"	23 000
$^9\text{Be}^+$ , lin. # 5	280	c.o.m.	3 - 10	"	35 000
$^9\text{Be}^+$ , lin. # 6	365	c.o.m.	3.5 - 10	"	11 000
$^{198}\text{Hg}^+$ , spherical	450	c.o.m	3	6	18

**Table 2.** Heating rates for various traps and various motional modes. For details on the spherical trap see [23, 4], while details on the Boulder traps for  $\text{Be}^+$  and  $\text{Hg}^+$  ions are found in [20, 9] and [24].

with the trap frequencies  $\omega^{-1}$ , and calculate the normalized heating rate  $\dot{N}$  at 1 MHz which is equivalent to an absorbed power. As seen from table 2, both  $\text{Ca}^+$  ion traps show very low normalized heating rates. As discussed in ref. [20], the heating rate may well depend on the distance  $d$  between the electrode surface and the ion-crystal with the fourth power  $d^4$ . For a discussion of the proposed  $d^4$ -dependence, we scale the normalized heating rate with the given distance and yield the proportionality coefficient for the law  $\dot{N} = c \cdot d^4[\text{mm}]$ , which takes a value of  $c = 2.4(1.5)$  for the spherical  $\text{Ca}^+$  Paul trap, 47(38) for the linear  $\text{Ca}^+$  trap and 164(38) for  $\text{Be}^+$  if only c.o.m. modes are averaged (120(83) for the overall average). Regarding the large standard deviation of all values, it seems to be still quite difficult to compare quantitatively the heating rates for different traps and ions in order to identify a common mechanism.

## 7. Sympathetic cooling

In this section we focus on the sympathetic nature of the ground state cooling technique described above. For state detection (section 4, step (iv)) we use the electron shelving technique, illuminating the complete ion string with light at 397 nm and 866 nm, and detecting the overall fluorescence. Ions in the  $S_{1/2}$  level scatter light on the dipole transition to the  $P_{1/2}$  state, while no fluorescence is observed if the ions have been excited into the  $D_{5/2}$  state. If we spatially adjust the laser at 729 nm into the centre of the ion-crystal, we observe a triple-peaked histogram as shown in fig. 6a. The maxima near 19, 48 and 79 photons correspond to - *no ion* in the  $S_{1/2}$  state, background light only, - *one ion* of the two in  $S_{1/2}$  and - *both ions* in  $S_{1/2}$  [21]. A histogram is built up from many 100 shot experiments, each shot having a detection time of 11.8 ms.

If the 729 nm laser is illuminating only one of the two ions, adjusted in a similar way as for the cooling of the two-ion-crystal, we observe a double-peaked histogram. Now,

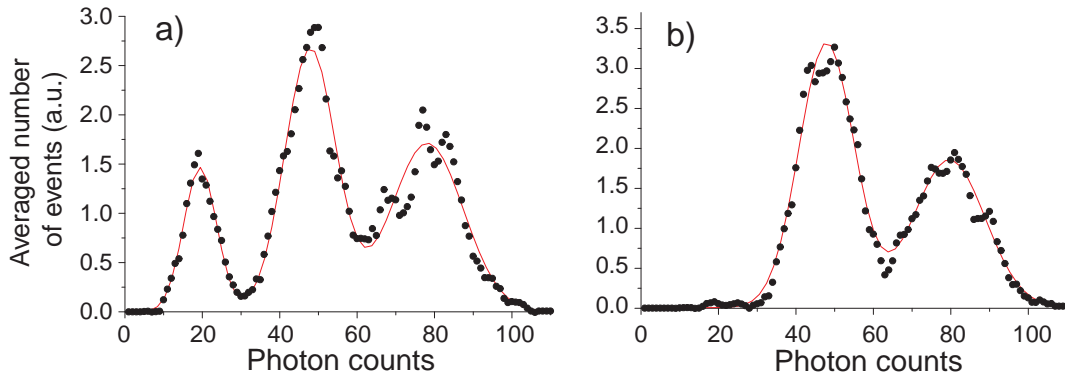


**Figure 6.** Both histograms are the averaged sum of many 100 shot experiments. Histogram (a) exhibits three peaks: one for no ionic excitation (far right peak), one ion excited (middle) and both ions excited (far left). Histogram (b) is collected with the laser addressing only one ion. It is clear that the peak corresponding to two ion excitation has disappeared.

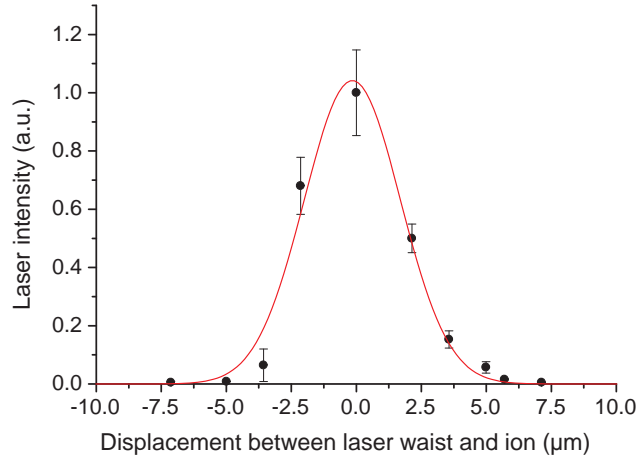


**Figure 7.** The width of the laser beam, as measured by exciting a single ion in the trap and observing Rabi oscillations. The waist,  $w_{cool}$ , is  $3.7\mu\text{m}$ .

only the second maximum near 48 and the third near 79 photons are visible (fig. 6b). With the laser focused on one of the ions only, it is impossible to excite both ions into the nonfluorescing  $D_{5/2}$  state, therefore the first peak in the histogram vanishes.

In a second measurement, with a single trapped ion in the linear trap, we deduced the waist size of the addressing beam at 729 nm. For this, we varied the position of the laser beam (in the axial direction) with respect to the ion position and excited Rabi oscillations on the  $S_{1/2} - D_{5/2}$  carrier transition. The measured Rabi frequency maps the electric field amplitude directly and we plot in fig. 7 the data together with a Gaussian fit which yields a  $3.7(0.2)\mu\text{m}$  waist size. For the axial trap frequency of 700 kHz we calculate [3] a two-ion separation of  $7.6\mu\text{m}$ . The measured laser intensity  $7\mu\text{m}$  away from the centre (location of the non-illuminated ion) is  $5 \cdot 10^{-3}$  in magnitude lower than that in the centre of the addressing beam focus.

## 8. Coherent dynamics on the qubit transition

With a two-ion-crystal cooled to the ground state as described in section 5, we have performed coherent manipulation on the qubit transition. Previously, in our group, we have cooled single ions [4, 22] and demonstrated coherent excitation on the qubit transition. Here we present results on the electronic state of a two-ion-crystal. We excite the carrier of the qubit transition after positioning the exciting laser in-between the two ions rather than illuminating only one of them. Rather than using a probe pulse of constant duration and power and varying the frequency, we keep the frequency and power constant and vary the duration. This way we build up a picture in time of the coherent dynamics of the electronic states of each ion. In the detection time, we need to set two thresholds in order to distinguish between one and two ions having been excited. As can be seen from the histogram (fig. 6) these thresholds can be placed accurately to distinguish the three possible states of the combined atomic population

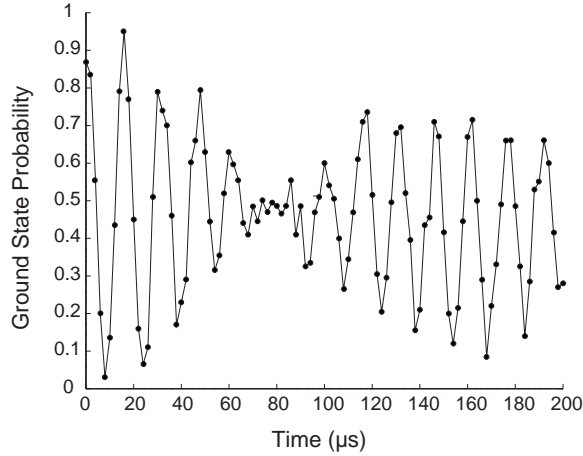


**Figure 8.** Rabi oscillations of two ions. Experimental data are shown as points and have been joined by lines to guide the eye. Note that the y axis is the probability of both ions being found in the non-excited state. The collapse and revivals of the combined atomic population indicate that we have created the states  $|\uparrow\downarrow\rangle$  and  $|\uparrow\uparrow\rangle$  from the starting state  $|\downarrow\downarrow\rangle$ .

when probed. The laser-ion interaction, with the laser frequency tuned to the carrier transition, will be described by different Rabi frequencies,  $\Omega_{Rabi}$ , of each ion. This means that the population of each ion will cycle with those different rates resulting in a coherent transfer from the  $S_{1/2}$  ground state and the  $D_{5/2}$  metastable state. These two frequencies  $\Omega_{Rabi}$  will "beat" with each other when considering the combined atomic population in the lower excited state. In this way, states such as  $|\uparrow\downarrow\rangle$  are generated, where a  $\downarrow(\uparrow)$  indicates that an ion is in the lower(upper) electronic state. If the spectator modes contained many phonons it would not be possible to see this effect. With our four sideband cooling and small Lamb-Dicke parameters we are able to observe the single bit rotations (implemented on the two ions) with high contrast. In fig. 8, at  $t = 0$  both ions are in the ground electronic state  $|\downarrow\downarrow\rangle$ . At  $t \sim 75 \mu s$  the signal has 'collapsed' to 0.5. This means that one ion has done an integer number of cycles up and down whereas the other ion has undergone an extra half cycle up, thus we have prepared the state  $|\uparrow\downarrow\rangle$ . Now the reappearance of the contrast occurs and at  $t \sim 155 \mu s$  both ions have been prepared in the upper electronic state,  $|\uparrow\uparrow\rangle$ . If there were no decoherence or heating mechanisms, then the signal would not deteriorate, however laser phase and magnetic field fluctuations cause the contrast in the Rabi oscillations to be lost.

We have demonstrated sympathetic ground state motional cooling of an ion chain with clear scaling possibilities to longer chains. We have cooled the chain on all four motional sidebands and achieved over 95% ground state populations in all the motional modes. From these ground state populations, we have measured the heating rates for various modes and found a typical rate of the order of  $10 \text{ phonons s}^{-1}$ . The measured heating rates in our trap are very favourable for the preparation of the motional ground state of an ion chain and its subsequent use as a quantum information processor.

This is in stark contrast to other measurements where the normalized heating rate has been found a factor of 1000 higher. By coherently exciting the qubit transition we could demonstrate the preparation of product states of the two ion chain. Our method of sympathetic motional ground state cooling relies on the ability to individually manipulate single ions which is also necessary for many suggested QC and quantum error correction schemes. The application of this technique will allow us to generate entanglement and implement quantum gates between ions in a chain.

This work is supported by the Austrian "Fonds zur Förderung der wissenschaftlichen Forschung" within the project SFB15 and in parts by the European Commission within the TMR networks "Quantum Information" (ERB-FMRX-CT96-0087) and "Quantum Structures" (ERB-FMRX-CT96-0077) and the "Institut für Quanteninformation GmbH".

- [1] J. I. Cirac and P. Zoller, Phys. Rev. Lett. **74**, 4091 (1995)
- [2] C. A. Sackett *et al.*, Nature **404**, 256 (2000)
- [3] H. C. Naegerl *et al.*, Phys. Rev. A **61** 023405 (2000)
- [4] Ch. Roos *et al.*, Phys. Rev. Lett. **83**, 4713 (1999)
- [5] R. J. Hughes *et al.*, Fortschr. Physik **46**, 329 (1998)
- [6] C. J. S. Donald *et al.*, e-print physics/0003085 (2000)
- [7] E. Peik *et al.*, Phys. Rev. A **60**, 439 (1999)
- [8] H. C. Naegerl *et al.*, Phys. Rev. A **60**, 145 (2000)
- [9] B. E. King *et al.*, Phys. Rev. Lett. **81**, 1525 (1998)
- [10] J. J. Bollinger, W. M. Itano, D. J. Wineland and D. J. Heinzen, Phys. Rev. A **54**, R4649
- [11] D. Kielpinski *et al.*, Phys. Rev. A **61**, 032310 (2000)
- [12] G. Morigi and H. Walther, e-print quant-ph/0005082 (2000)
- [13] W. Paul, Z. Naturforsch. **A8**, 448 (1953)
- [14] D. J. Berkeland, J. D. Miller, J. C. Bergquist, W. M. Itano, and D. J. Wineland, J. Appl. Phys. **83**, 5025 (1998)
- [15] D. V. F. James, Applied Physics B **66**, 181, (1998)
- [16] A. Steane, Appl. Phys. B **64**, 632, (1997)
- [17] D. Reiss, A. Lindner and R. Blatt, Phys. Rev. A **54**, 5133 (1996)
- [18] D. J. Wineland and W. M. Itano, Phys. Rev. A **20**, 1521 (1979).
- [19] C. A. Blockley and D. F. Walls and H. Risken, Europhys. Lett. **17**, 509 (1992), I. Cirac and R. Blatt and A. S. Parkins and P. Zoller, Phys. Rev. Lett. **70**, 762 (1993), for a review see: D. J. Wineland *et al.*, J. Res. Natl. Inst. Stand. Technol., **103**, 259 (1998)
- [20] Q. A. Turchette *et al.*, Phys. Rev. A **61**, 063418, (2000)
- [21] After opening the vacuum chamber, we noticed the photomultiplier observation viewport to be heavily coated with Ca which reduced the overall count rate by at least a factor of 3.
- [22] F. Schmidt-Kaler *et al.*, to appear in J. Mod. Opt., e-print quant-ph/0003096 (2000)
- [23] Ch. Roos, Ph.D. Thesis, Universität Innsbruck, (2000) unpublished
- [24] F. Diedrich, J. C. Bergquist, W. M. Itano and D. J. Wineland, Phys. Rev Lett. **62**, 403 (1989); C. Monroe *et al.*, Phys. Rev. Lett. **75**, 4011 (1995)